Gastric Cancer
DOI 10.1007/s10120-013-0334-y

ORIGINAL ARTICLE

In vivo optical pathology of paclitaxel efficacy on the peritoneal metastatic xenograft model of gastric cancer using two-photon laser scanning microscopy

Tadanobu Shimura · Koji Tanaka · Yuji Toiyama · Masato Okigami · Shozo Ide · Takahito Kitajima · Satoru Kondo · Susumu Saigusa · Masaki Ohi · Toshimitsu Araki · Yasuhiro Inoue · Keiichi Uchida · Yasuhiko Mohri · Akira Mizoguchi · Masato Kusunoki

Received: 15 September 2013 / Accepted: 22 December 2013

Abstract
Background We previously visualized in vivo responses to chemotherapy in a colorectal liver metastatic xenograft model using in vivo real-time and time-series intravital two-photon laser scanning microscopy (TPLSM). In this study, we established the method for evaluating the response of peritoneal xenografts to chemotherapy of metastatic gastric cancer using intravital TPLSM.
Methods Red fluorescent protein-expressing gastric cancer cells (NUGC4) were inoculated into the peritoneal cavity of green fluorescent protein nude mice.
Results Laparotomy revealed that 2 weeks after inoculation, macroscopic peritoneal metastatic nodules were formed. The first intravital TPLSM session revealed that they were composed of red tumor cell clusters and green surrounding stroma. Paclitaxel was administered intraperitoneally after the first TPLSM three times a week for 7 days in the treatment group. At the second laparotomy, there were significantly fewer and smaller nodules in the treated mice than in the controls. The second intravital TPLSM session showed tumor cell fragmentation, swelling, and nuclear condensation in the metastatic nodules—a response to chemotherapy. There were multinuclear tumor cells in the paclitaxel-treated living mice.
Conclusions Our method may become a powerful tool for evaluating the efficacy of novel anti-gastric cancer drugs in a preclinical murine model with minimum interindividual variation.

Keywords Paclitaxel · Peritoneal metastatic xenograft · Gastric cancer · Two-photon laser scanning microscopy

T. Shimura (✉) · K. Tanaka · Y. Toiyama · M. Okigami · S. Ide · T. Kitajima · S. Kondo · S. Saigusa · M. Ohi · T. Araki · Y. Inoue · K. Uchida · Y. Mohri · M. Kusunoki
Department of Gastrointestinal and Pediatric Surgery, Mie University Graduate School of Medicine, 2-174 Edobashi, Tsu, Mie 514-8507, Japan
e-mail: t-shimura@clin.medic.mie-u.ac.jp

A. Mizoguchi
Department of Neural Regeneration and Cell Communication, Mie University Graduate School of Medicine, Tsu, Mie, Japan

Introduction

Peritoneal metastasis of gastric cancer indicates a poor prognosis. According to the nationwide registry of the Japanese Gastric Cancer Association, the 5-year survival rates for P1 patients was 8.3 %, which was significantly inferior to that for P0 patients (74.5 %) [1]. Systemic chemotherapy is the main treatment for gastric cancer with peritoneal metastasis, but a standardized regimen has not been established [2]. In the case of peritoneal metastasis, intraperitoneal (i.p.) chemotherapy appears to be efficient because the anti-cancer drugs are delivered directly into the peritoneal cavity, where they maintain a high concentration.

Paclitaxel is an anti-cancer drug that was isolated from the plant *Taxus brevifolia* (western yew tree) [3]. Paclitaxel promotes microtubule assembly [4]. An in vitro study revealed that paclitaxel inhibits cell mitosis by arresting growth mainly in the G_2/M phases of the cell cycle [5].

After i.p. administration, paclitaxel remains in the peritoneal cavity for a relatively long time because of its high molecular weight and hydrophobicity [6–8]. Studies have shown that i.p. administration of paclitaxel is effective in the treatment of gastric cancer with peritoneal metastasis [9–11].

Two-photon laser scanning microscopy (TPLSM) has made it possible to visualize living tissues intravitally

Published online: 08 January 2014

because of its high-resolution and high-magnification imaging, increased tissue penetration, and minimal phototoxicity to and photobleaching of living cells. Single-photon confocal laser scanning microscopy does not have these features [12–14]. Thus, TPLSM has been widely used and has become an important tool in the field of tumor biology [15–18].

We developed a method for intravital TPLSM imaging with high resolution and high magnification. It was made possible by reducing microvibrations in the observational area caused by heartbeats and respiratory movements using an organ-stabilizing system (Japanese Patent Application number: P2007-129723) [19, 20]. We also established a time-series TPLSM technique consisting of multiple time points for intravital TPLSM observations (time-series TPLSM) in the same living mice over periods of days to months. The animals comprised a dextran sulfate sodium-induced colitis model [21] and a colorectal liver metastases model [22, 23]. We evaluated in vivo and in real time the response to chemotherapy given for colorectal xenografts of liver metastatic tumor to study the dynamic interactions between metastatic tumor cells and host stromal cells in living mice [24].

In this study, we aimed to establish a means of visualizing the response to chemotherapy in a xenograft model of metastatic gastric cancer in the peritoneum using in vivo real-time TPLSM and in vivo time-series TPLSM.

Materials and methods

Green fluorescent protein (GFP)-expressing nude mice

GFP-expressing nude mice (C57BL/6-BALB/c-nu/nu-EGFP) were purchased from AntiCancer Japan (Osaka, Japan). GFP nude mice (20–22 g) were bred, housed in groups of six mice per cage, and fed with a pelleted basal diet (CE-7; CLEA Japan, Tokyo, Japan). The mice had free access to drinking water. They were kept in the animal house facilities at Mie University School of Medicine under standard conditions of humidity (50 ± 10 %), temperature (23 ± 2 °C), and light (12/12 h light/dark cycle) according to the Institutional Animal Care Guidelines. The experimental protocols were reviewed and approved by the Animal Care and Use Committee at the Mie University Graduate School of Medicine.

Red fluorescent protein (RFP)-expressing human gastric cancer cell line

RFP expressing the human gastric cancer cell line (RFP-NUGC4) was purchased from AntiCancer Japan (Osaka, Japan). RFP-NUGC4 cells were grown in monolayer cultures in RPMI 1640 (Sigma-Aldrich, St. Louis, MO, USA) supplemented with fetal bovine serum 10 % (vol/vol) (GIBCO BRL, Tokyo, Japan), glutamine (2 mM), penicillin (100,000 units/L), streptomycin (100 mg/L), and gentamicin (40 mg/L) at 37 °C in a 5 % CO_2 environment. For routine passage, cultures were spilt 1:4 when they reached 90 % confluence, generally every 5 days. Cells at the third to sixth passage were used for peritoneal metastasis experiments, which were performed with exponentially growing cells.

Chemotherapeutic agent

Paclitaxel was purchased from Sigma-Aldrich. The stock solutions of the drug were made in dimethylsulfoxide and then dissolved in appropriate concentrations using distilled water for the in vivo study. To monitor the response to chemotherapy in peritoneal metastatic xenografts, paclitaxel (10 mg/kg i.p.) was administered three times a week for 7 days (treatment group). In the control group, phosphate-buffered saline (PBS) was injected i.p. according to the same protocol.

Murine peritoneal metastasis model

RFP-NUGC4 cells at the third to sixth passage were harvested with trypsin/EDTA and washed in serum-containing RPMI 1640 medium to inactivate any remaining trypsin. The RFP-NUGC4 cells were then centrifuged and resuspended in PBS. Then, the cells were adjusted to 1×10^8 cells/mL for single-cell suspensions. Finally, 5×10^7 cells were inoculated into the peritoneal cavity of GFP nude mice using a 30-gauge needle.

Surgical procedure for intravital TPLSM

A middle-portion midline laparotomy was undertaken as short as possible (<15 mm). The small bowel, mesentery, and omentum were exteriorized through the laparotomy incision to identify the peritoneal metastatic nodules. After identifying the nodules, the exteriorized organs distant from the nodules were put back into the abdominal cavity to prevent bowel dehydration. The metastatic nodules that had developed on the mesentery or omentum were positioned on the caudal part of the surgical incision to minimize the influence of heartbeats and respiratory movement during intravital TPLSM (Fig. 1a). The nodules were suitably placed on a wet gauze to keep them moist (Fig. 1b). They were fixed between the solder lug terminal and the wet gauze using an organ-stabilizing system (Fig. 1c) (Japanese Patent Application number P2007-129723). The organ stabilizer minimized the microvibrations of the observed area so we could obtain a clear, high-resolution image of the intra-

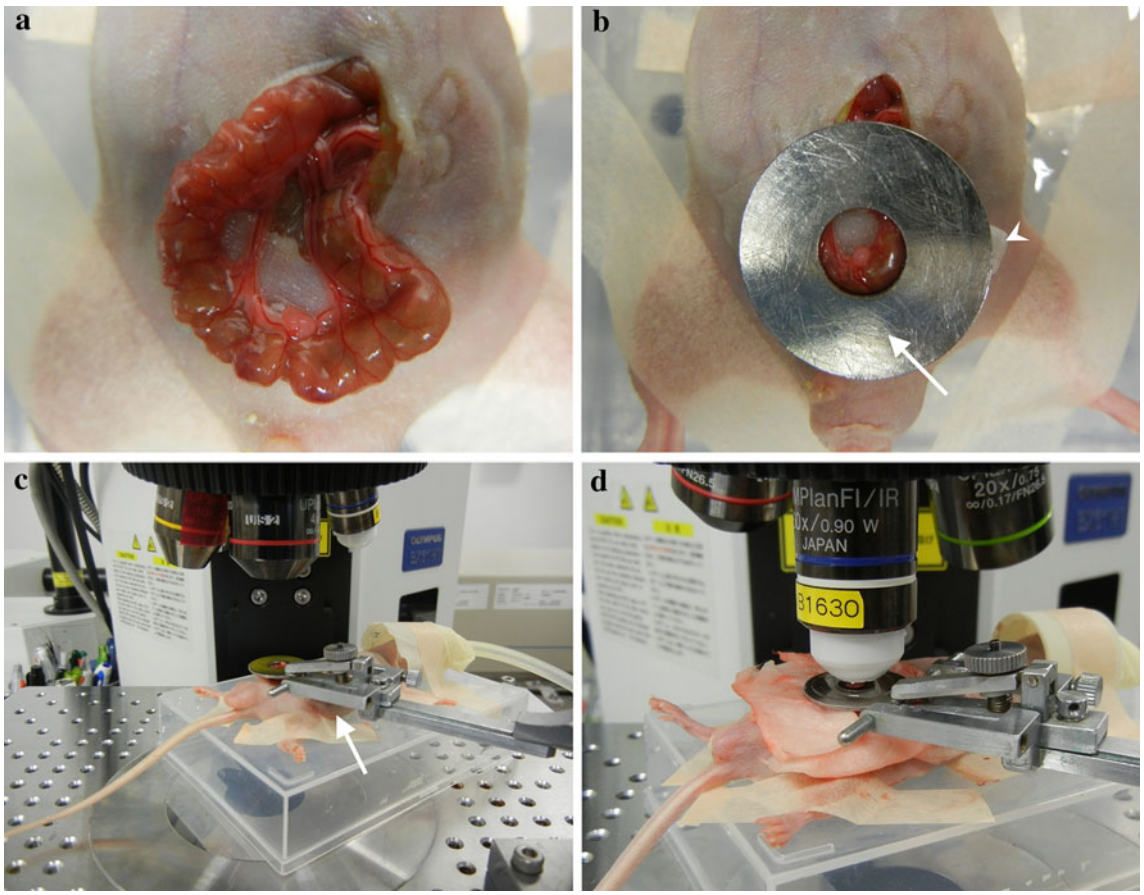

Fig. 1 Overview of peritoneal metastatic nodule fixation and intravital TPLSM setup. **a** The peritoneal metastatic nodule developed on the mesentery were exteriorized. **b** The nodule was placed between a solder lug turminal (*arrow*) and a wet gauze (*arrowheads*). **c** The nodule was fixed using an organ stabilizing system (*arrow*). **d** After intravital TPLSM at a lower magnification, the nodule was observed at a higher magnification (water-immersion)

abdominal organs [19]. Such stabilization and fixation of the metastatic nodules were most important and technically the most difficult part of the intravital TPLSM procedure. After applying PBS to the observed area, a thin cover glass was placed gently on the surface of the nodules. After this first intravital TPLSM session, the exteriorized metastatic nodules were placed back in the abdominal cavity. Sodium hyaluronate and a carboxymethylcellulose membrane (Seprafilm Adhesion Barrier; Genzyme Corporation, Cambridge, MA, USA) was placed between the nodules and the abdominal wall to prevent postoperative dense adhesion. PBS (400–500 μL) was administered into the abdominal cavity before abdominal closure to prevent dehydration after surgery. The duration of this surgical procedure, including the TPLSM, should be 1 h (at most) to minimize surgical stress.

TPLSM setup

The procedures for TPLSM setup were performed as described elsewhere [22]. Experiments were done using an upright microscope (BX61WI; Olympus, Tokyo, Japan) and an FV1000-2P laser-scanning microscope system (FLUOVIEW FV1000MPE; Olympus). The use of special stage risers enabled the unit to have an exceptionally wide working distance, which allowed the stereotactically immobilized, anesthetized mouse to be placed on the microscope stage. The microscope was fitted with water-immersion optics as well as several lenses that had high numerical apertures to provide the long working distances required for in vivo work. The excitation source in TPLSM mode was Mai Tai Ti:sapphire lasers (Spectra Physics, Mountain View, CA, USA), which was tuned and mode locked at 910 nm. The Mai Tai produces light pulses of about 100 fs width (repetition rate 80 MHz). Laser light reached the sample through the microscope objectives connected to an upright microscope (BX61WI; Olympus). The mean laser power at the sample was between 10 and 40 mW, depending on the depth of imaging. Microscope objective lenses used in this study were 4× UPlanSApo (numerical aperture 0.16), 10× UPlanSApo (numerical aperture 0.4), and 60× LUMPlanFI/IR (water dipping, numerical aperture 0.9, working distance

2 mm). Data were analyzed using an FV10-ASW (Olympus). TPLSM images were acquired with 512 × 512 pixels spatial resolution, 210 μm field of view dimension, and a pixel dwelling time of 4 μs. An internal detector (non-descanned detection method) collected the two-photon fluorescence signals at an excitation wavelength that enabled simultaneous acquisition of the enhanced green fluorescent protein (EGFP) and RFP (DsRed2) signals. An excitation wavelength of 1050 nm is optimum for DsRed2, as reported by Kawano et al. [25], whereas an excitation wavelength of 910 nm is optimum for EGFP. Therefore, it is difficult to excite DsRed2 sufficiently at 910 nm. To overcome this difficulty, we adjusted the detection sensitivity (brightness by HV) manually for EGFP (450–500) and DsRed2 (550–600) to promote optimal simultaneous imaging of EGFP and DsRed2.

Imaging peritoneal metastasis of gastric cancer using intravital TPLSM

The surface of the peritoneal nodules were initially screened at lower magnifications by setting out the *X*/*Y* plane and adjusting the *Z* axis manually to detect the optimal observation area containing RFP-expressing cancer cells (in at least three areas). Each area of interest was subsequently scanned at a higher magnification (water-immersion objective 60×, with or without 2× zoom) by manually setting the *X*/*Y* plane and adjusting the *Z* axis (automatically or manually) to obtain high-resolution clear TPLSM images. The scanning areas were 200 × 200 μm (600×) or 100 × 100 μm (600×, with 2× zoom). The imaging depth or imaging stack was determined arbitrarily to allow real-time three-dimensional visualization of peritoneal metastases of gastric cancer in vivo. The laser power was adjusted according to the imaging depth. When imaging at larger depths, we increased the laser power level (up to 100 %) manually using the laser power level controller. For optimal simultaneous imaging of EGFP and RFP (DsRed2), detection sensitivity (brightness by HV) was adjusted manually for EGFP (450–500) or RFP (550–600), respectively.

Time-series imaging using intravital TPLSM

Intravital TPLSM was performed before and after paclitaxel administration for imaging peritoneal metastatic lesions in the same living mouse. A sodium hyaluronate and carboxymethylcellulose membrane (Seprafilm Adhesion Barrier; Genzyme Corporation, Cambridge, MA, USA) was useful for preventing the formation of postoperative adhesions between the peritoneal metastatic nodules and the abdominal wall. Precautions to prevent postoperative intraperitoneal infection were taken during the entire surgical procedure of time-series intravital TPLSM.

Experimental schedule for time-series intravital TPLSM

After i.p. inoculation of RFP-NUGC4 cells into GFP nude mice, macroscopic peritoneal metastases of gastric cancer were observed by 2 weeks. The first intravital TPLSM session was scheduled 2 weeks after inoculation to confirm the presence of peritoneal metastatic lesions. After that, paclitaxel (10 mg/kg i.p.) was administered three times a week for 7 days in the treatment group. In the control group, PBS was injected i.p. according to the same protocol. The second intravital TPLSM was performed after paclitaxel administration to observe the in vivo real-time response to chemotherapy in the tumor microenvironment of peritoneal metastatic xenografts of gastric cancer in the same living mice. These mice were imaged at two time points by time-series intravital TPLSM. At the end of the experiments (after the second intravital TPLSM session), the peritoneal nodules in the mesentery or omentum were harvested and subjected to histopathological analysis (Fig. 2).

Quantification of morphologically changed tumor cells as paclitaxel treatment response at the second TPLSM session

At the second intravital TPLSM session, at least five areas containing RFP-NUGC4 cells were observed at higher magnifications. The percentages of morphologically changed cells (the response to paclitaxel treatment) in an observation area of 200 × 200 μm were scored as follows: 0 (<5 %), 1 (6–25 %), 2 (26–50 %), 3 (51–75 %), 4 (>76 %) (Fig. 5). The score for each mouse was defined as the mean value of each observational area's score. Comparison of the score (mean ± standard deviation) in the control group ($n = 5$) and the paclitaxel treatment group ($n = 5$) was performed by statistical analysis using the Mann–Whitney's U test. $p < 0.05$ was considered to indicate significance.

Hematoxylin-eosin staining of metastatic nodules

Harvested peritoneal nodules were fixed in 2 % paraformaldehyde for 24 h at 4 °C and then transferred to 25 % sucrose for 24 h at 4 °C. After that, the nodules were transferred to tissue cryo-molds coated with Tissue-Tek O.C.T. compound medium (Sakura Finetek USA, Torrance, CA, USA). The prepared samples were sliced at a thickness of 5 μm with a Microm HM 505 E cryostat (Microm, Walldorf, Germany), and the sections were placed on silane-coated slides. After air drying for 30 min, conventional hematoxylin-eosin staining was performed.

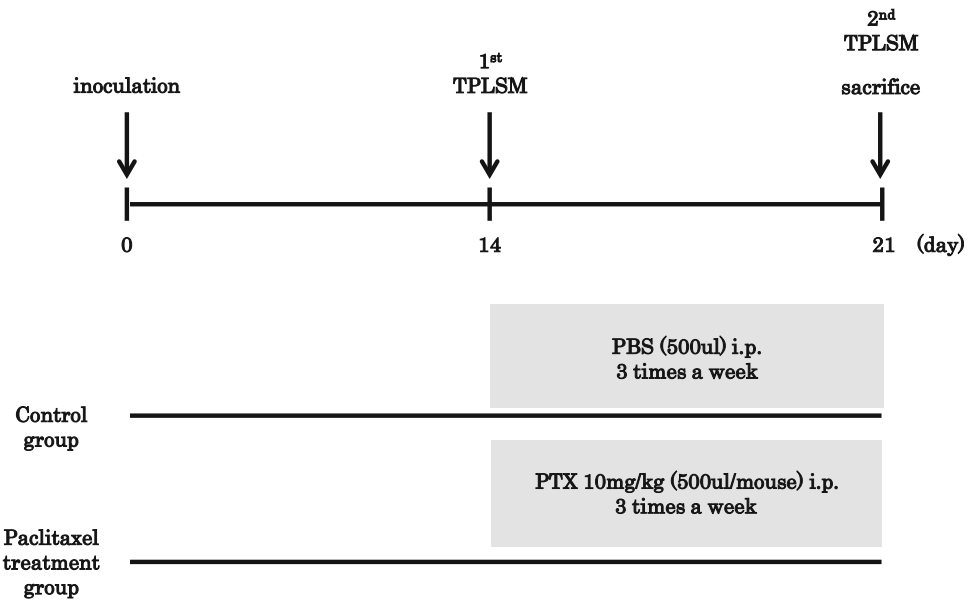

Fig. 2 Timing of intravital imaging. The first TPLSM session took place 2 weeks after inoculation. Paclitaxel (10 mg/kg i.p.) was then administered three times a week for 7 days. At the second intravital TPLSM session (7 days after paclitaxel administration), the same mice were subjected to in vivo visualization of any pathology due to the response to chemotherapy. It focused on assessment of the microenvironment of nodules on the peritoneal metastatic xenografts. *TPLSM* two-photon laser scanning microscopy, *PTX* paclitaxel

Results

Macroscopic metastatic nodule formation on metastatic gastric cancer xenografts

Two weeks after inoculation of 5×10^7 RFP-NUGC4 cells into the peritoneal cavity of GFP nude mice, RFP-NUGC4 cells had formed macroscopic peritoneal metastatic nodules on the mesentery or the omentum of GFP nude mice (Fig. 4a, c). Approximately 80 % of all mice inoculated with 5×10^7 RFP-NUGC4 cells had macroscopic peritoneal metastatic nodules.

Peritoneal metastases at the first intravital TPLSM session

Macroscopic peritoneal metastatic nodules were composed of red tumor cell clusters and the green areas in the surrounding stroma at the first intravital TPLSM session. Abnormally tortuous tumor vessels were observed around peritoneal metastatic lesions composed of RFP-NUGC4 cells at lower magnifications (×40–100) (Fig. 3a, b). At higher magnifications (>×600), the nuclei and cytoplasm of RFP-NUGC4 cells were clearly visible (Fig. 3c, d).

Macroscopic effect of paclitaxel on peritoneal metastatic xenografts

After the first intravital TPLSM session was completed, either paclitaxel (treatment group) or PBS (controls) was administered. The size and the number of peritoneal metastatic nodules in the control group were significantly greater than those in the paclitaxel treatment group (Fig. 4b). In the treatment group, some of the metastatic nodules had shrinked or disappeared macroscopically, (Fig. 4d). We measured the weight of the harvested and stocked frozen samples of peritoneal nodules from the mesentery or omentum. The weight (mean ± standard deviation) of nodules in the PTX treatment group ($n = 5$) was significantly less (0.13 ± 0.09 g) than that in the control group ($n = 5$) (0.79 ± 0.34 g) ($p = 0.012$).

In vivo response to chemotherapy by peritoneal metastatic xenografts at the second intravital TPLSM session

The second intravital TPLSM session—scheduled to follow the first TPLSM and paclitaxel treatment—was undertaken to observe the in vivo real-time response of the tumor and the host's microenvironment to chemotherapy in the same living mice. There were no marked morphological changes in the metastatic nodules of the control mice (Fig. 5a). In contrast, the treatment group exhibited an in vivo response to chemotherapy that included tumor cell fragmentation, swelling, and nuclear condensation (Figs. 5b–e, 6d). There were also no marked changes in the host's microenvironment in vivo at this second intravital TPLSM session. Thus, there were no morphological changes or endothelial damaging to the tumor vessels, and no coagulation abnormalites (data not shown).

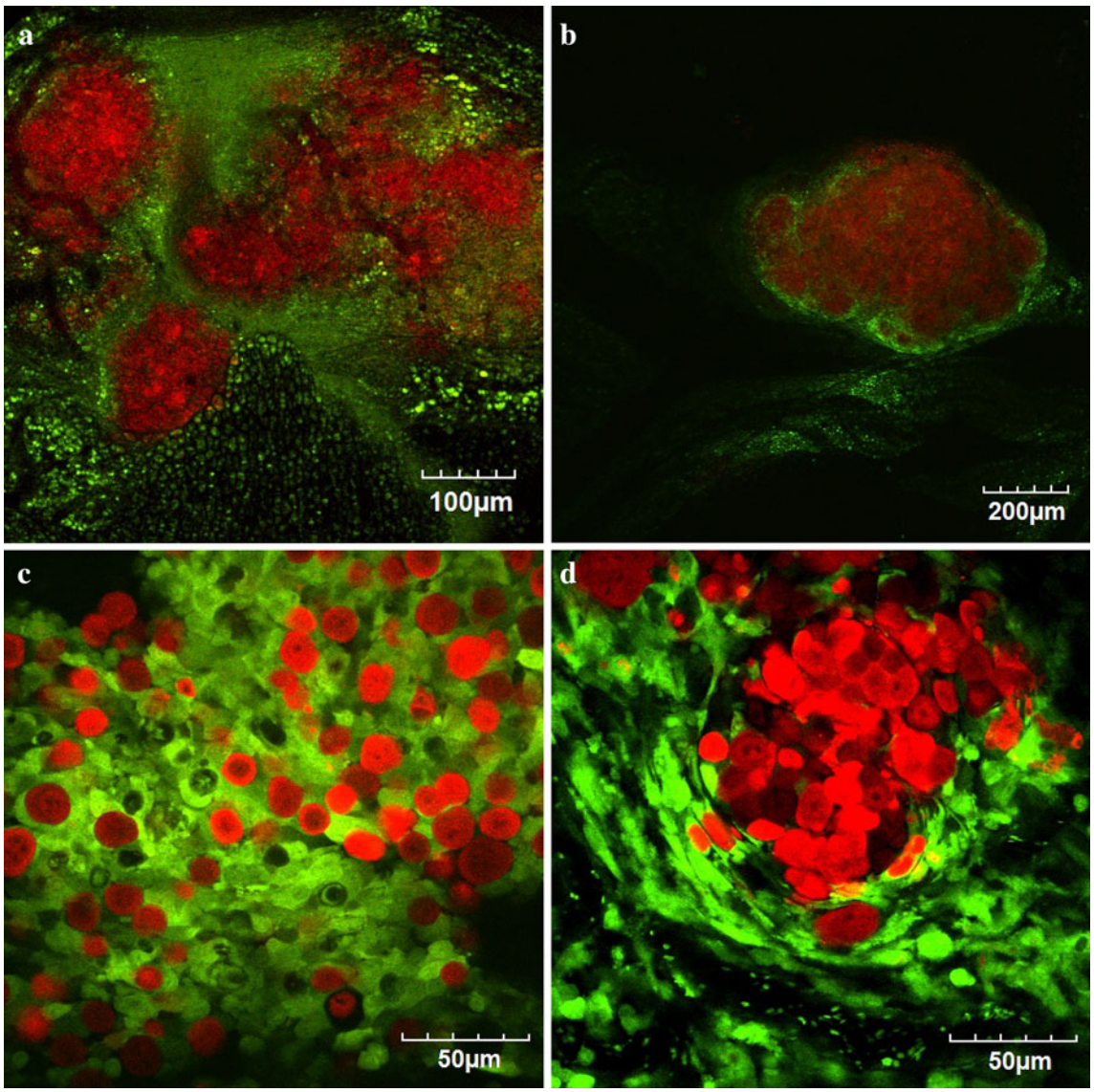

Fig. 3 Peritoneal metastases formed by the time of the first intravital TPLSM session. **a** Peritoneal metastases that had developed on the omentum (×100). **b** Peritoneal metastases that had developed on the mesentery (×40). **c**, **d** Peritoneal metastases at higher magnification (×600). Note the tumor cells (*red*) and the surrounding reactive stroma with tumor vessels (*green*)

Quantification of morphologically changed tumor cells in response to paclitaxel treatment at the second TPLSM session

The mean ± standard deviation for the control group was 0.81 ± 0.58, whereas that for the treatment group was 2.00 ± 0.72. These figures indicate that the frequency of morphological changes in the tumor cells occurred with significantly higher frequency in the treatment group ($p = 0.046$) (Fig. 5f).

Visualization of multinuclear cells at the second TPLSM

Multinuclear tumor cells were seen at the second intravital TPLSM session in some mice in the treatment group (Fig. 6a, b).

Hematoxylin-eosin staining of the metastatic nodules

In the control mice, most of the tumor cells in the metastatic nodules did not change morphologically (Fig. 5g). In

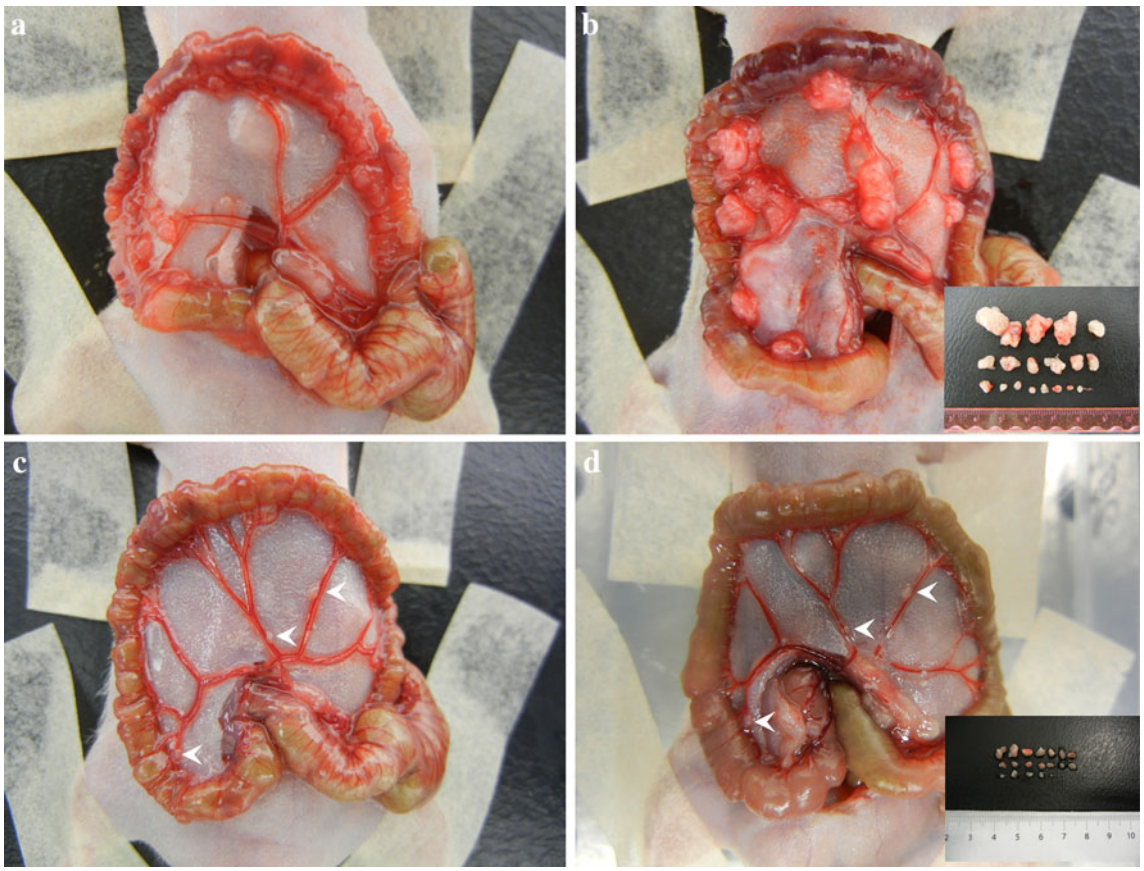

Fig. 4 Macroscopic response to paclitaxel chemotherapy aimed at peritoneal metastatic xenografts. **a** Macroscopic peritoneal metastases in a control mouse at the first intravital TPLSM session. **b** Growth of the peritoneal metastatic nodules in a control mouse at the second intravital TPLSM session. **c** Macroscopic peritoneal metastases (*arrowheads*) in a mouse in the treatment group at the first intravital TPLSM session. **d** Macroscopic changes in the peritoneal metastatic nodules (*arrowheads*) in a mouse in the treatment group at the second intravital TPLSM session. The size and the number of metastatic nodules were significantly smaller than those in the control mouse

contrast, tumor cell fragmentation, swelling, nuclear condensation, and apoptotic bodies were observed in some of the metastatic nodules of the treated mice (Figs. 5h, 6e). A few multinuclear cells were also observed in the treatment group (Fig. 6c).

Discussion

In our previous study, we were able to visualize in vivo and in real time the response to 5-fluorouracil or irinotecan chemotherapy for liver metastatic xenografts of colorectal cancer using time-series intravital TPLSM in the same mice [24]. In the present study, we have successfully established a method for evaluating the response to chemotherapy in peritoneal metastatic xenografts of gastric cancer using intravital TPLSM. Using our model, it was possible to perform in vivo real-time imaging of peritoneal metastases of gastric cancer at high optical resolution and magnification. It was also possible to perform time-series imaging to evaluate morphological changes in metastases after paclitaxel treatment.

It has been reported that morphological changes of tumor cells induced by administration of paclitaxel include tumor cell fragmentation, cell shrinkage, membrane blebbing, chromatin condensation, chromatin crescents, nuclear cleavage, and apoptotic body formation [26–28]. In this study, we found tumor cell fragmentation, shrinkage, and nuclear condensation as evidence of the efficacy of paclitaxel during the second intravital TPLSM session in the same living mice.

We also visualized multinuclear tumor cells in the living mice after paclitaxel treatment during the second intravital TPLSM session at high optical resolution and magnification. It is suggested that mitotic spindle checkpoint failure and aberrant mitotic exit are mechanisms for multinuclear cell formation. Mitotic stress induced by anticancer agents (e.g., paclitaxel) and irradiation also triggers formation of multinuclear cells [29]. Other evidence suggests that some of the multinuclear cells escape from apoptotic cell death and

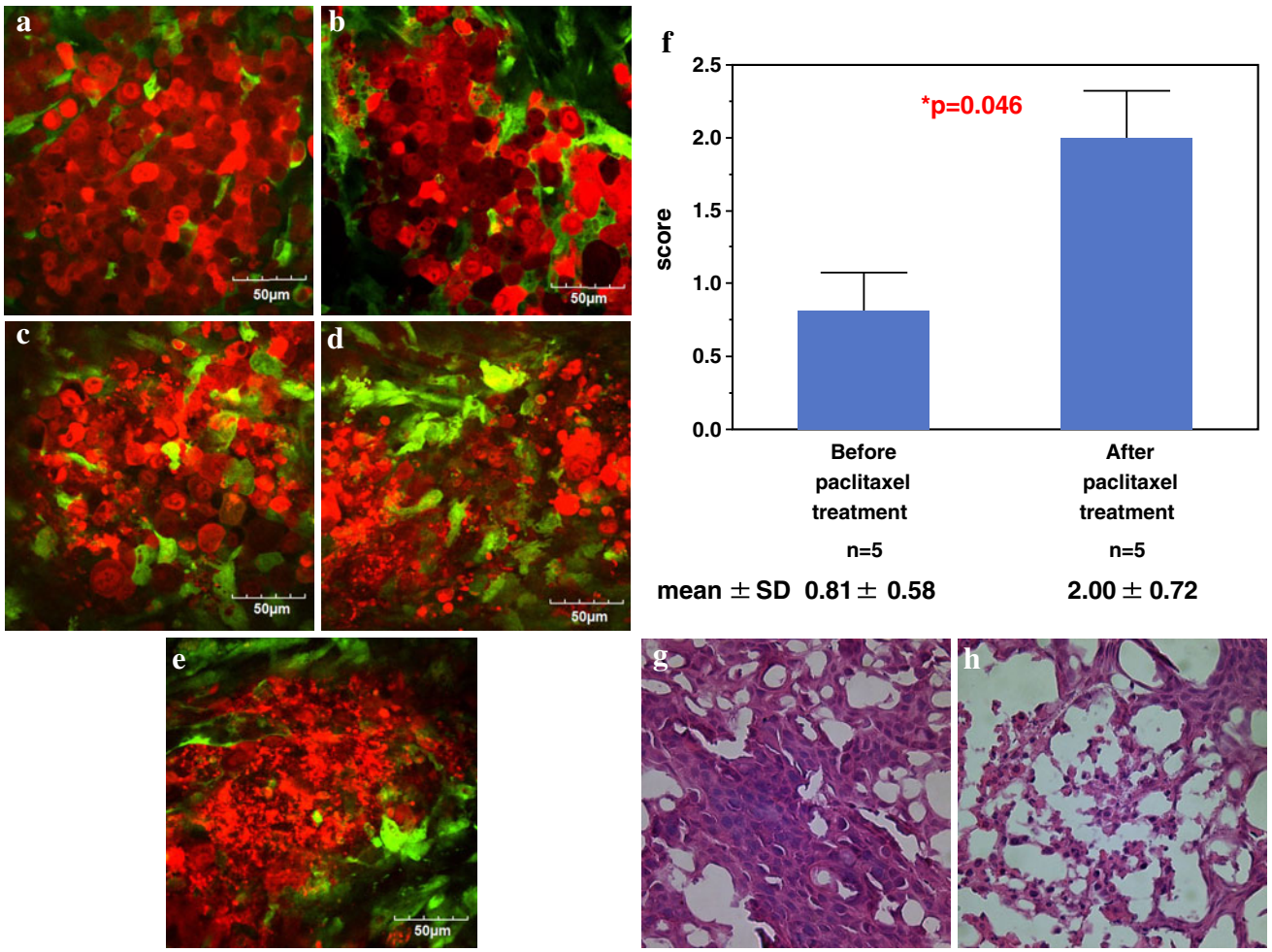

Fig. 5 Quantification of morphologically changed tumor cells as a response to paclitaxel treatment during the second TPLSM session. **a** Tumor cells of the metastatic nodules in a control mouse during the second intravital TPLSM (×600). **b–e** Tumor cells of the metastatic nodules in a paclitaxel-treated mouse during the second intravital TPLSM session (×600). Tumor cell fragmentation, swelling, and nuclear condensation were observed, representing the response to chemotherapy. At the second intravital TPLSM session, the percentage of morphologically changed tumor cells in response to paclitaxel treatment in a observed 200 × 200 μm area were scored as follows. **a** 0 (<5 %). **b** 1 (6–25 %). **c** 2 (25–50 %). **d** 3 (51–75 %). **e** 4 (>76 %). **f** The mean ± standard error in the control group was 0.81 ± 0.26, whereas that in the treatment group was 2.00 ± 0.32. Thus, the incidence of morphological change was significantly higher in the treatment group ($p = 0.046$). **g** Hematoxylin–eosin (H–E) staining of the peritoneal nodules in the control group (×400). **h** H–E staining of the peritoneal nodules in the treatment group (×400). Tumor cell fragmentation, nuclear condensation, and cell shrinkage were apparent

acquire the ability to survive [30, 31]. If so, multinuclear cell formation may be related to the development of cancer cell resistance to anti-cancer drugs such as paclitaxel [32].

We believe that the method of visualizing the histopathology of viable tumor cells described herein has several advantages over conventional histopathological examinations. First, we were able to clearly evaluate the dynamic pathology of viable tumor cells at the cellular level with high resolution and magnification. Second, because the peritoneal metastatic nodule can be rotated, we could also visualize multi-directional three-dimensional histopathological information about the viable tumor cell by adjusting the *Z* axis automatically or manually without the artifact of tissue shrinkage by fixation or tissue destruction by microtome sectioning. Third, our techniques for quantifying the morphologically changed tumor cells are useful for evaluating paclitaxel efficacy in living mice with higher quality imaging.

Our method also has several technical difficulties. (1) It was difficult to perform intravital TPLSM on metastatic peritoneal nodules in the subphrenic and retroperitoneal areas because of the difficulty exteriorizing these nodules. (2) The duration of the surgical procedure, including the first TPLSM session, had to be 1 h or less to minimize surgical stress if we planned to have the mice survive for the second TPLSM session. (3) At the second TPLSM

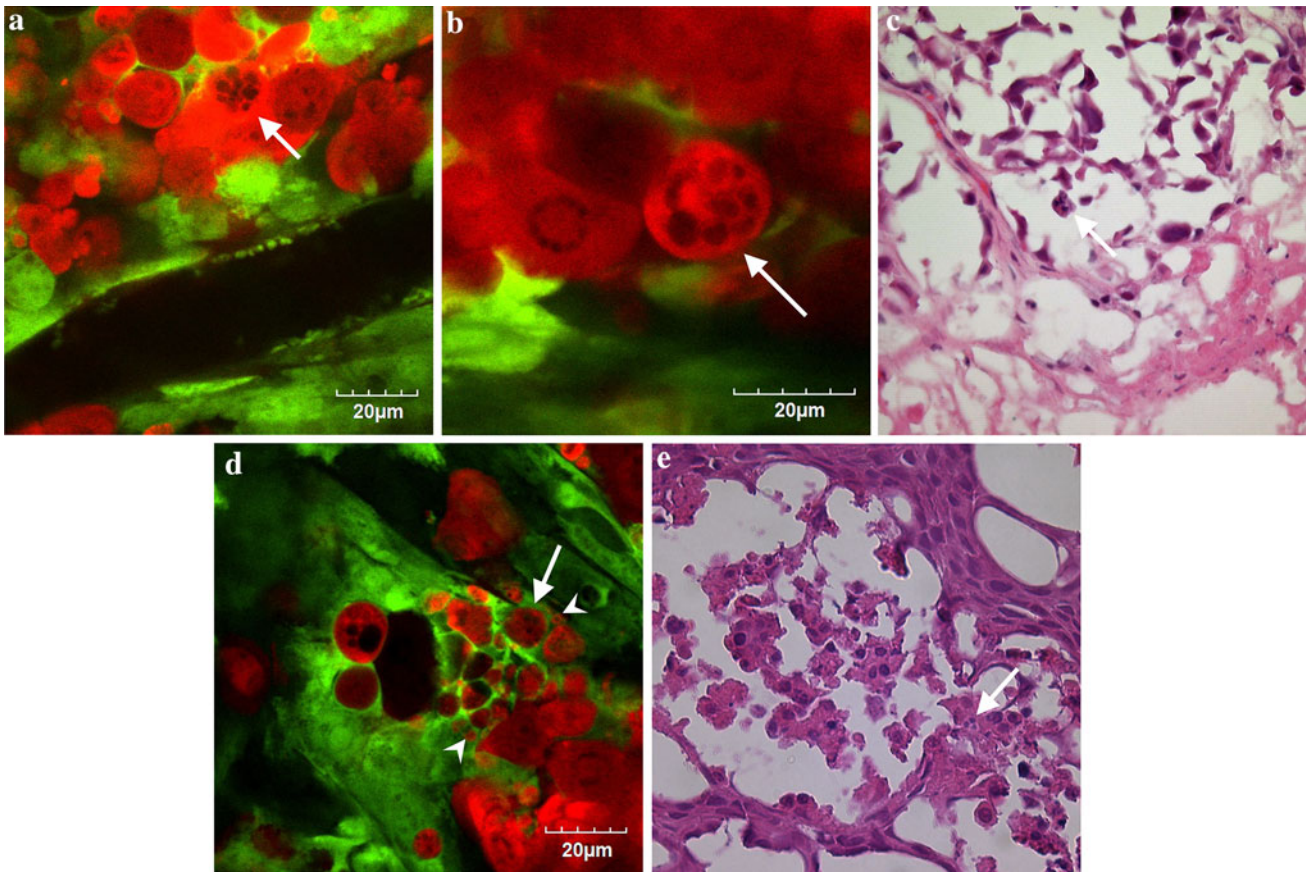

Fig. 6 Visualization of multinuclear cells at the second TPLSM session. Multinuclear cell (*arrow*) was visualized at higher magnification during intravital TPLSM. **a** ×1200. **B** ×1800. **c** Multinuclear cell (*arrow*) after H–E staining (×400). **d** Tumor cell shrinkage (*arrowheads*) and apoptotic body (*arrow*) were seen by intravital TPLSM (×1200). **e** Apoptotic body (*arrow*) after H–E staining (×400)

session, it was difficult to observe peritoneal metastatic nodules for more than 4–5 h because performing intravital TPLSM with the organ exteriorized subjected the mice to great surgical stress. Hence, with our present techniques, it is not possible to visualize "in vivo real-time morphological changing" in tumor cells in response to PTX i.p. therapy. Our method needs to be improved.

There is a site-specific variation in response to chemotherapy for a number of human malignant tumors [33]. We believe that metastatic xenografts are more practical than subcutaneous xenografts for evaluating the efficacy of novel anti-cancer chemotherapeutic agents.

Although our method needs some technical improvements, it is possible that intravital TPLSM of peritoneal metastatic xenografts of gastric cancer may become a useful tool for evaluating chemotherapy efficacy and the development of resistance to novel anti-gastric cancer chemotherapeutic agents.

In conclusion, we have established a method for evaluating the response to chemotherapy in peritoneal metastatic xenografts of gastric cancer using in vivo real-time and time-series intravital TPLSM. This technique may become a powerful tool for investigating the efficacy of novel antigastric cancer drugs in preclinical murine metastatic xenografts with minimum interindividual variation.

Acknowledgments This work was supported by grants from the Ministry of Education, Culture, Sports, Science and Technology of Japan (KAKENHI 25462052 to K.T.; 30586764 to M.K.).

Conflict of interest All of the authors declare no conflict of interest.

References

1. Nashimoto A, Akazawa K, Isobe Y, Miyashiro I, Katai H, Kodera Y, et al. Gastric cancer treated in 2002 in Japan: 2009 annual report of the JGCA nationwide registry. Gastric Cancer. 2013;16:1–27.
2. Koizumi W, Narahara H, Hara T, Takagane A, Akiya T, Takagi M, et al. S-1 plus cisplatin versus S-1 alone for first-line treatment of advanced gastric cancer (SPIRITS trial): a phase III trial. Lancet Oncol. 2008;9:215–21.

3. Wani MC, Taylor HL, Wall ME, Coggon P, McPhail AT. Plant antitumor agents. VI. The isolation and structure of taxol, a novel antileukemic and antitumor agent from Taxus brevifolia. J Am Chem Soc. 1971;93:2325–7.
4. Schiff PB, Fant J, Horwitz SB. Promotion of microtubule assembly in vitro by taxol. Nature. 1979;277:665–7.
5. Schiff PB, Horwitz SB. Taxol stabilizes microtubules in mouse fibroblast cells. Proc Natl Acad Sci USA. 1980;77:1561–5.
6. Eiseman JL, Eddington ND, Leslie J, MacAuley C, Sentz DL, Zuhowski M, et al. Plasma pharmacokinetics and tissue distribution of paclitaxel in CD2F1 mice. Cancer Chemother Pharmacol. 1994;34:465–71.
7. Mohamed F, Marchettini P, Stuart OA, Yoo D, Sugarbaker PH. A comparison of hetastarch and peritoneal dialysis solution for intraperitoneal chemotherapy delivery. Eur J Surg Oncol. 2003;29:261–5.
8. Ohashi N, Kodera Y, Nakanishi H, Yokoyama H, Fujiwara M, Koike M, et al. Efficacy of intraperitoneal chemotherapy with paclitaxel targeting peritoneal micrometastasis as revealed by GFP-tagged human gastric cancer cell lines in nude mice. Int J Oncol. 2005;27:637–44.
9. Fushida S, Furui N, Kinami S, Ninomiya I, Fujimura T, Nishimura G, et al. Pharmacologic study of intraperitoneal paclitaxel in gastric cancer patients with peritoneal dissemination. Gan To Kagaku Ryoho. 2002;29:2164–7.
10. Ishigami H, Kitayama J, Otani K, Kamei T, Soma D, Miyato H, et al. Phase I pharmacokinetic study of weekly intravenous and intraperitoneal paclitaxel combined with S-1 for advanced gastric cancer. Oncology. 2009;76:311–4.
11. Ishigami H, Kitayama J, Kaisaki S, Hidemura A, Kato M, Otani K, et al. Phase II study of weekly intravenous and intraperitoneal paclitaxel combined with S-1 for advanced gastric cancer with peritoneal metastasis. Ann Oncol. 2010;21:67–70.
12. Kobat D, Durst ME, Nishimura N, Wong AW, Schaffer CB, Xu C. Deep tissue multiphoton microscopy using longer wavelength excitation. Opt Express. 2009;17:13354–64.
13. Wang BG, Konig K, Halbhuber KJ. Two-photon microscopy of deep intravital tissues and its merits in clinical research. J Microsc. 2010;238:1–20.
14. Ustione A, Piston DW. A simple introduction to multiphoton microscopy. J Microsc. 2011;243:221–6.
15. Kienast Y, von Baumgarten L, Fuhrmann M, Klinkert WE, Goldbrunner R, Herms J, et al. Real-time imaging reveals the single steps of brain metastasis formation. Nat Med. 2010;16:116–22.
16. Le Devedec SE, van Roosmalen W, Pont C, Lalai R, de Bont H, van de Water B. Two-photon intravital multicolour imaging to study metastatic behaviour of cancer cells in vivo. Methods Mol Biol. 2011;769:331–49.
17. Beerling E, Ritsma L, Vrisekoop N, Derksen PW, van Rheenen J. Intravital microscopy: new insights into metastasis of tumors. J Cell Sci. 2011;124:299–310.
18. Textor J, Peixoto A, Henrickson SE, Sinn M, von Andrian UH, Westermann J. Defining the quantitative limits of intravital two-photon lymphocyte tracking. Proc Natl Acad Sci USA. 2011;108:12401–6.
19. Toiyama Y, Mizoguchi A, Okugawa Y, Koike Y, Morimoto Y, Araki T, et al. Intravital imaging of DSS-induced cecal mucosal damage in GFP-transgenic mice using two-photon microscopy. J Gastroenterol. 2010;45:544–53.
20. Koike Y, Tanaka K, Okugawa Y, Morimoto Y, Toiyama Y, Uchida K, et al. In vivo real-time two-photon microscopic imaging of platelet aggregation induced by selective laser irradiation to the endothelium created in the beta-actin-green fluorescent protein transgenic mice. J Thromb Thrombolysis. 2011;32:138–45.
21. Morimoto Y, Tanaka K, Toiyama Y, Inoue Y, Araki T, Uchida K, et al. Intravital three-dimensional dynamic pathology of experimental colitis in living mice using two-photon laser scanning microscopy. J Gastrointest Surg. 2011;15:1842–50.
22. Tanaka K, Morimoto Y, Toiyama Y, Okugawa Y, Inoue Y, Uchida K, et al. Intravital dual-colored visualization of colorectal liver metastasis in living mice using two photon laser scanning microscopy. Microsc Res Tech. 2012;75:307–15.
23. Tanaka K, Morimoto Y, Toiyama Y, Matsushita K, Kawamura M, Koike Y, et al. In vivo time-course imaging of tumor angiogenesis in colorectal liver metastases in the same living mice using two-photon laser scanning microscopy. J Oncol. 2012;2012:265487.
24. Tanaka K, Okigami M, Toiyama Y, Morimoto Y, Matsushita K, Kawamura M, et al. In vivo real-time imaging of chemotherapy response on the liver metastatic tumor microenvironment using multiphoton microscopy. Oncol Rep. 2012;28:1822–30.
25. Kawano H, Kogure T, Abe Y, Mizuno H, Miyawaki A. Two-photon dual-color imaging using fluorescent proteins. Nat Methods. 2008;5:373–4.
26. Chang YF, Li LL, Wu CW, Liu TY, Lui WY, P'Eng FK, et al. Paclitaxel-induced apoptosis in human gastric carcinoma cell lines. Cancer. 1996;77:14–8.
27. Zhou HB, Zhu JR. Paclitaxel induces apoptosis in human gastric carcinoma cells. World J Gastroenterol. 2003;9:442–5.
28. Stepien A, Grzanka A, Grzanka D, Andrzej Szczepanski M, Helmin-Basa A, Gackowska L. Taxol-induced polyploidy and cell death in CHO AA8 cells. Acta Histochem. 2010;112:62–71.
29. Long BH, Fairchild CR. Paclitaxel inhibits progression of mitotic cells to G1 phase by interference with spindle formation without affecting other microtubule functions during anaphase and telephase. Cancer Res. 1994;54:4355–61.
30. Jordan MA, Toso RJ, Thrower D, Wilson L. Mechanism of mitotic block and inhibition of cell proliferation by taxol at low concentrations. Proc Natl Acad Sci USA. 1993;90:9552–6.
31. Illidge TM, Cragg MS, Fringes B, Olive P, Erenpreisa JA. Polyploid giant cells provide a survival mechanism for p53 mutant cells after DNA damage. Cell Biol Int. 2000;24:621–33.
32. Kim SM, Kim R, Ryu JH, Jho EH, Song KJ, Jang SI, et al. Multinuclear giant cell formation is enhanced by down-regulation of Wnt signaling in gastric cancer cell line, AGS. Exp Cell Res. 2005;308:18–28.
33. Talmadge JE, Singh RK, Fidler IJ, Raz A. Murine models to evaluate novel and conventional therapeutic strategies for cancer. Am J Pathol. 2007;170:793–804.